Available online at www.sciencedirect.com

ScienceDirect

Geochimica et Cosmochimica Acta 212 (2017) 119–132

Geochimica et Cosmochimica Acta

www.elsevier.com/locate/gca

Changes in the As solid speciation during weathering of volcanic ashes: A XAS study on Patagonian ashes and Chacopampean loess

G. Bia [a], M.G. García [a,b], L. Borgnino [a,b,*]

[a] Centro de Investigaciones en Ciencias de la Tierra (CICTERRA), CONICET - UNC, Argentina
[b] FCEFyN Universidad Nacional de Córdoba, Córdoba, Argentina

Received 1 March 2017; accepted in revised form 9 June 2017; Available online 15 June 2017

Abstract

X-ray absorption spectroscopy (XAS) was used to determine the oxidation state of As, local chemical coordination and the relative proportion of different As species in recent and ancient Andean volcanic ashes, as well as in Chaco Pampean loess. As K edge XANES analysis indicates that in loess sediments the dominant species is As(V) (i.e., >91%). Conversely, As(III) is dominant in all ash samples. In the Puyehue sample, only As(III) species were determined, while in both, the Chaitén and the ancient tephra samples, As(III) species accounts for 66% of the total As. The remaining 34% corresponds to As(−1) in the Chaitén sample and to As(V) in the weathered tephra. The proposed EXAFS models fit well with the experimental data, suggesting that in ancient and recent volcanic ashes, As(III) is likely related to As atoms present as impurities within the glass structure, forming hydroxide species bound to the Al-Si network. In addition, the identified As(−1) species is related to arsenian pyrite, while in the ancient volcanic ash, As(V) was likely a product of incipient weathering. In loess sediments, the identified As(V) species represents arsenate ions adsorbed onto Fe oxy(hydr)oxides, forming inner-sphere surface complexes, in a bidentate binuclear configuration.

Keywords: XAS; As solid speciation; Al-silicate glass; South America

1. INTRODUCTION

The presence of elevated concentrations of Arsenic (As) in both surface and groundwater sources in South America represents one of the most important environmental issues in the region. The prolonged intake of waters with elevated concentrations of As results in the well-known symptoms of chronic As poisoning, known in Argentina as Chronic Endemic Regional Hydroarsenicism (in Spanish: "Hidroarsenicismo Crónico Regional Endémico - HACRE"). The Chaco-Pampean plain of Argentina is the largest area in the world (about 1 million km^2) with high As concentrations in groundwater (Bundschuh et al., 2012 and reference therein). While in Argentina the disease was first described in the early 20th century, the illness had been present since the Precolumbian Era (Arriaza et al., 2010). In the Andean region of northern Chile, arsenicosis has also been recognized as a disease that affected the earliest inhabitants (about BC 7000 and BC 2000), as evidenced by the high concentration of As found in hair, bones and skin of preserved mummies (Byrne et al., 2010; Rivadeneira et al., 2010; Kakoulli et al., 2014; Swift et al., 2015).

For decades, a great number of studies were conducted to better understand the natural sources of this hazardous pollutant, and the factors that control its mobility in the

* Corresponding author at: Av. Vélez Sarsfield 1611, X5016GCA Córdoba, Argentina.
E-mail address: lauraborgnino@gmail.com (L. Borgnino).

http://dx.doi.org/10.1016/j.gca.2017.06.016
0016-7037/

aquatic reservoirs. Previous works (Nicolli et al., 1989; Bundschuh et al. 2004; Bhattacharya et al., 2006; Sracek et al., 2009; Nicolli et al., 2010; Nicolli et al., 2012) described volcanic glass spread within the loess matrix as the primary natural source of As. While the primary and secondary sources of As in groundwater were mostly inferred on the basis of water geochemistry analysis, only a few works identified the As-bearing phases associated with loess sediments (Smedley et al., 2005; Nicolli et al., 2010; Borgnino et al., 2013; García et al., 2014). In fact, there are just a few studies reporting the chemical composition of glasses separated from loess (e.g., Nicolli et al., 1989; Nicolli et al., 2010). Recently, Bia et al. (2015) used fresh volcanic ashes collected after recent eruptions of Patagonian volcanoes as proxies for glass grains spread within loess. In this work, the authors identify the presence of As(III)-S and As(V)-O species on the glass surfaces, that were formed by chemical reactions occurring in the volcanic plume during the eruption, as well as by alteration during transport. The release of As from these coatings depends on the solubility of the As-bearing compounds and the physico-chemical conditions that predominate during transport and in the deposition location. However, the presence of As in volcanic glasses is not restricted to the above-mentioned coatings. In one of the pioneering works that characterized the solid speciation of As atoms in natural glasses, Borisova et al. (2010) reported the occurrence of oxy-hydroxide complexes, such as $AsO(OH)_2^-$ and $As(OH)_3$ in rhyolitic peraluminous glasses. The identification of the second shell of coordination (or neighboring) could not be resolved in this work; however the authors proposed that this position should be restricted to a bond via one oxygen atom to the Al-Si network of the glass, or coordinated to the major cations K/Na via electrostatic attraction in the disordered glass structure. The importance of defining the type and strength of bonds between As and the neighboring atoms lies in the control that these bondings exert on the As release during glass alteration.

Although the literature related to the As sources in the Chaco Pampean loess is abundant (Smedley and Kinniburgh, 2002; Bundschuh et al., 2004; Smedley et al., 2005) the solid speciation of As has not yet been addressed. Results of selective extraction carried out with loess samples revealed that an important fraction of As in the sediment is associated with Fe and Mn oxy(hydr)oxides (Smedley et al., 2005; Sracek et al., 2009). In view of the oxidizing conditions dominating in groundwater of the region, such association should likely represent As(V) atoms (i.e., arsenate) sorbed onto these oxides. Therefore, if the speciation and coordination of As in volcanic ash and loess are different, there is an oxidation stage that should transform the As(III) within the glass structure to the As(V) specie in the loess sediments. This stage still remains to be unraveled.

In recent decades, X-ray absorption spectroscopy (XAS) analysis have gained attention in Geoscience due to the increasing ability of beamlines to determine trace concentrations at high spatial resolutions (Alexandratos et al., 2007; Fernández-Martínez et al., 2008; Chakraborty et al., 2010; Aurelio et al., 2010). Nevertheless, XAS studies concerning the analysis of As in geological samples are still scarce (Savage et al., 2000; Zielinski et al., 2007; Borisova et al. 2010; Essilfie-Dughan et al., 2013; Root et al., 2015; Wang et al., 2016).

The purpose of this work is to contribute to the understanding of the As redox transformations that occur when volcanic ash is exposed to the Earth surface conditions for prolonged time periods. The oxidation state and the local chemical coordination of As and Fe in recently emitted ashes (the past eight years), ancient ashes (~125,000 years) and loess sediments have been determined by synchrotron XAS at the K-edges of As and Fe. Specifically, for loess samples, the junction analysis of the As and Fe elements allowed for the discrimination of the As-bearing compounds present in the sample.

2. MATERIALS AND METHODS

2.1. Volcanic ashes and loess sediments

The occurrence of discrete tephra layers, along with high contents of volcanic shards within the loess, is the result of direct contributions of volcaniclastic particles emitted during the past Andean volcanic eruptions (Zárate, 2003; Tripaldi et al., 2010). These volcanic materials were supplied from eruptive centers located along the Central and Southern volcanic zones (CVZ and SVZ, respectively). The two volcanic arcs, located in western South America, are separated by volcanically inactive gaps, where subduction is at such a shallow angle that magma is not generated (Global Volcanism Program, Smithsonian Institution). The volcanic eruptions of the Southern Volcanic Zone are more significant as a source of loess material in the southern Pampas, while the volcanoes of the Puna plateau were probably the main source of loess in the Chaco region and in some of the northern Pampas tephras (Zárate, 2003).

Recently emitted volcanic ash samples were collected a few hours after the eruptions of the Chilean volcanoes Chaitén (May 2nd, 2008; 42°S72°W) and Puyehue (June, 3rd-6th-2011, 40°S 72°W). The Chaitén sample was collected in the village of Esquel (Argentina), located about 110 km E of the volcano, while the Puyehue sample was collected from the roof of a house in the city of Bariloche (Argentina), located 90 km SE from the volcano. The ancient tephra (T) was collected from a ~10 cm thick layer of tephra found in an exposed profile along provincial road No. 65 (Buenos Aires Province, 36°52′S; 62°14′W; 115 m a.s.l.). This layer is embedded in a fluvial fine sand deposit partially cemented with calcium carbonates. The base of the deposit is not exposed but based on the regional context, it likely overlies the late Miocene sediments that outcrop at a short distance in the Encadenadas lakes and constitute the general substrate of the region (Zárate and Tripaldi, 2012; Lorenzo et al., 2013). The ashes are overlain by a shallow mantle of fine aeolian sands. On the basis of its stratigraphic position, it is assumed that the tephra layer could be a Pleistocene deposit *sensu lato*, likely older than late Pleistocene (i.e., older than 125 ka B.P). Loess sample L-1 was collected from the bottom of a 12 m profile exposed in an abandoned road excavation at Corralito

(Córdoba Province; 32°00′S; 64°09′W; 490 m a.s.l.), 35 km south of the city of Córdoba. The sedimentological characteristics of this profile are described elsewhere (Frechen et al., 2009). Sample L-10 was collected from a 5 m deep borehole located in the city of Lamadrid (Tucumán Province; 27°38′S; 65°14′W; 293 m a.s.l), 90 km south of the city of San Miguel de Tucumán.

After collection, samples were air-dried and sieved through <63 μm mesh in order to separate the more frequent grain-size fractions, which are lower than 63 μm in all cases (Kröhling, 1999; Bia et al., 2015).

2.2. Chemical characterization

The chemical and mineralogical characteristics of the ashes emitted during the eruptions of the Chaitén and Puyehue volcanoes, as well as those of the two loess samples, have been described elsewhere (Borgnino et al., 2013; García et al., 2014; Bia et al., 2015). The bulk chemical composition of the ancient volcanic ash was determined by ICP-OES (SpectroCiros Vision) after lithium metaborate/tetraborate fusion (NF ISO 14869-2), while As was determined by ICP-MS (Perkin Elmer 5000) after aqua regia total digestion. The validity of the results for major, minor, and trace elements was checked against measurement of OREAS45EA and STD SO-19 standards, which were carried out along with sample analysis.

2.3. XAS data collected

XAS spectra (including X-ray absorption near-edge structure region or XANES and extended X-ray absorption fine structure region or EXAFS) of the ashes, loess and reference patterns of As/Fe-bearing solids were collected at the XAFS2 beamline of the Laboratório Nacional de Luz Síncrotron (LNLS), in Campinas, Brazil. The beamline was equipped with a monochromator consisting of double crystal Si (1 1 1), and the electron storage ring was operated at 1.37 GeV with a current range of about 110–300 mA. Spectra were collected at room temperature in transmission mode for As and Fe reference materials, and in fluorescence mode for the studied samples.

As K-edge XAS spectra were collected over the energy range between 11,790 and 12,600 eV. The monochromator step size was 1.0–2.0 eV per step; however in the XANES region (11,850–11,930 eV) it was reduced to 0.5 eV per step, which ensures higher resolution spectra. Fe K-edge XAS spectra were collected over the energy range between 7020 and 8000 eV. The monochromator step size was 2.0–3.0 eV per step and it has been reduced to 0.3 eV per step between 7090 and 7200 eV. For As measurements, energy was calibrated using a gold metallic foil and setting the first inflection point to the energy of the Au L3 absorption edge (11,919 eV) while for Fe measurements, energy was calibrated using an Fe metallic foil standard and setting the K-edge energy at 7112 eV. The stability of the beamline was monitored during sample measurements with the corresponding reference behind the samples.

For XAS data collection, samples were ground to fine-grained powders while reference materials were diluted with reagent-grade boron nitride at the ratio of 1:6. Then, 70 mg of the diluted references materials and 400–600 mg of the <63 μm grain-size fraction of the samples were mechanical pressed to obtain pellets. For measurements, the pellets were fixed onto acrylic holders and sealed with a Kapton tape film. Five scans, each one with a duration of 58 min, were collected for the analyzed samples, while three scans, each one with a duration of 23 min, were collected for the reference compounds. At the end of every two scans, the beam position was changed in order to avoid beam-induced spectral modifications to the samples. Additionally, the obtained spectra were compared in order to check possible shifting occurring during measurements. Natural As- and Fe-bearing reference solids, such as native arsenic (As^0), arsenopyrite (FeAsS), orpiment (As_2S_3), realgar (As_4S_4), scorodite ($FeAsO_4$ $2H_2O$), pyrite (FeS_2), illite ($(K,H_3O)(Al,Mg,Fe)_2(Si,Al)_4O_{10}[(OH)_2,(H_2O)]$) and goethite (α-FeOOH) were obtained from the CICTERRA mineral collection. Other analytical grade reagents, such as Na-arsenate ($Na_2HAsO_4{\cdot}7H_2O$), As_2O_3 and Na-arsenite ($NaAsO_2{\cdot}4H_2O$) were also used as reference material. In addition, a reference material corresponding to As co-precipitated on Fe(hydr)oxides was prepared by mixing 0.3 M $Fe(NO_3)_3$ and 0.2 M $Na_2HAsO_4{\cdot}7H_2O$ solutions at pH ~ 7.5 (Waychunas et al., 1993; Fuller et al., 1993). The pH was regulated by the slow addition of 6.0 M NaOH.

2.3.1. XAS data analysis

EXAFS analysis was used to extract data information about the identity, coordination and radial distance of atoms in the first and second shells around the target central atom (i.e., As/Fe). In the simplest case, each peak in the Fourier Transformed (FT) graph represents the correlation between one type of absorber-backscatter pair (e.g.: As/Fe and O). However, EXAFS analysis of complex and heterogeneous materials, such as geological samples, may become more complicated due to the presence of overlapping peaks, multi-atom shells, increased disorder due to the presence of poorly crystalline phases, and decreased data quality due to background fluorescence from Fe, which is usually concentrated in such materials (Foster et al., 1998). As a general rule, when EXAFS is used to discriminate between multiple chemical species of the same element, at least 10% of one species is needed (Foster et al., 1998). Low concentrations of the target atom lead to low signal-to-noise patters in the EXAFS region of the spectra. This is the case of the ashes and loess samples analysed in this work, where the As concentrations vary between 2.4 and 40 μg g^{-1}. To overcome this challenge, XANES spectra were first analyzed by comparing the major peaks position in first derivate spectra and then each phase was quantified by linear combination fit (LCF) analysis. The information obtained from XANES and LCF were then used to perform the EXAFS modeling.

XANES and EXAFS spectra were analyzed using the Athena and Artemis software based on the IFEFFIT computer package (Ravel and Newville, 2005) and following the recommendations of the International XAFS Society (Sayers, 2000). Briefly, spectra normalization and

background removal were performed in each of the sample's scans and then merged in energy space using Athena. The value corresponding to the first derivate spectra maximum was assigned to the edge energy value (E_0).

Calculations involved in LCF were conducted with the Athena software, which apply a non-linear least-squares minimization over the range of energy spanning from 11,840 to 11,920 eV in normalized XANES spectra. The sum of contributions from each fitted phase accounted for 100 in terms of percentage, while ΔE was not allowed to vary due to previous calibration of the spectra. The quality of the fit was assessed on the basis of the *R* factor and χ^2 values provided by Athena software. LCF analysis was carried out using some selected reference phases in order to determine the contributions of the As(-1)-S, As(III)-O in silicates and As(V)-O species. The proportion of As(-1) was quantified using FeAsS as a reference material, while the contribution of As(III)-O species was determined on the basis of the Macusani glass spectrum, reported by Borisova et al. (2010) and provided by the authors. The contributions of As(V)-O species was determined using the synthesized As(V)-coprecipitated on Fe-(hydr)oxide compounds.

To fit the FT data, the theoretical phase shift and the scattering amplitude parameters were calculated by means of FEFF 6.0 ab-initio code (Zabinsky et al., 1995) included in the IFFEFIT package (Ravel and Newville, 2005). Fits were performed in the *R*- and *k*-space to obtain the identity of the backscattering atoms, the interatomic distance (*R*) between the As/Fe and the dispersant atom, the coordination number (*N*) and the mean-square disorder parameter (Debye-Waller parameter, σ^2). Samples fittings were performed using *k*3 weighting.

Theoretical backscattering amplitude and phase-shift functions for the pair absorber-backscatterer As/Fe-O/X (where X is Si/Na/Al), were computed using the crystal structures of AsFeS (Fuess et al., 1987), As_2O_3 (Pertlik, 1978), $Na_2HAsO_4{\cdot}H_2O$ (Baur and Khan, 1970), vesuvianite (Groat et al., 2013), FeS_2 (Elliot, 1960), muscovite (Guggenheim et al., 1987), scorodite (Hawthorne, 1976) and goethite (Gualtieri and Venturelli, 1999). The amplitude reduction factor (S_0^2) was set at 0.75 ± 0.05 and was obtained by fitting experimental spectra of the crystalline standard (As_2O_3). This value was used then in all data fits. The remaining variable parameters for each shell (i.e., *N*, *R* and σ^2) were fixed or floated during fitting after assigning a reasonable starting value. Fixed N values were used for the standard compounds fitting, because they have known crystallographic data while for the studied samples *N*, *R* and σ^2 were floated. Depending on data quality, normalized spectra were fitted over a k-range of 3–11 $Å^{-1}$ while R-ranges is encompassed between 1.1 and 4.0 Å (not corrected for backscatterer phase shift).

2.4. Sequential extraction

Sequential extractions were performed in recent ashes in order to identify the following phases: (1) water soluble; (2) strongly adsorbed As; (3) As bound to Fe (III) oxyhydroxides (i.e., ferrihydrite, schwertmannite, etc.); and (4) As bound to primary sulfides. The As content that remained in the residual fraction was calculated as $[As]_{near\text{-}total} - \Sigma[As]_{steps1\text{-}4}$ and assigned to the fraction of As associated with silicates. The details of the procedure are described as Supplementary Material (see SI1).

3. RESULTS

3.1. Chemical composition of volcanic ashes and loess sediments

Table 1 shows the bulk chemical composition of the analyzed samples. For the three volcanic ashes, the contents of SiO_2 and $Na_2O + K_2O$ range between 68.6–72.5 wt% and 7–8 wt% respectively. Therefore, according to the TAS classification (Le Maitre, 1984) Chaitén ashes are dacitic/rhyolitic in type; Puyehue ashes show a trachydacitic composition, and T ashes are rhyolitic. Loess samples are andesitic in type according to their alkalis and silica contents.

The As concentrations in both loess sediment samples are rather similar (15–16 μg g^{-1}), while in volcanic ashes, As concentrations are more variable (2.4–40 μg g^{-1}). A similar trend can be observed when analysing Fe concentrations: while in loess samples Fe contents (expressed as Fe_2O_3) are similar (4.9 and 5.4 wt%), in the volcanic ashes the Fe concentrations vary between 1.3 and 4.4 wt%. Conversely, the concentrations of Al (expressed as Al_2O_3) show scarce variability, ranging from 12.64 and 15.94 wt%.

3.2. XANES analysis

3.2.1. As speciation

Normalized As XANES spectra and first derivative analysis of samples and reference materials are shown in Fig. 1 and SI2, respectively. Major peaks in first derivative spectra are listed in Table 2. As a general rule, the inflection

Table 1
Bulk chemical composition of the studied samples determined by ICP/OES.

Samples	Chaitén[a]	Puyehue[a]	T	L-1[b]	L-10[b]
Chemical composition (%)					
SiO_2	72.45	68.62	70.62	58.6	61.24
Al_2O_3	13.88	13.27	12.64	15.01	15.94
$Fe_2O_{3(T)}$	1.81	4.4	1.29	4.9	5.41
Na_2O	4.07	5.2	4.09	2.23	2.49
CaO	1.74	2.05	0.88	4.51	2.57
K_2O	2.88	2.82	4.13	2.76	3.39
MgO	0.46	0.65	0.64	1.65	2.35
TiO_2	0.175	0.599	0.22	0.708	0.786
MnO	0.067	0.111	0.06	0.097	0.092
P_2O_5	0.09	0.09	0.04	0.23	0.14
LOI	ND	ND	ND	6.90	4.60
Total	97.6	97.8	100.00	97.6	99.0
As concentration (μg g^{-1})					
	40.0	15.0	2.4	16	15

ND, not determined.
[a] Data from Bia et al. (2015).
[b] García et al. (2014).

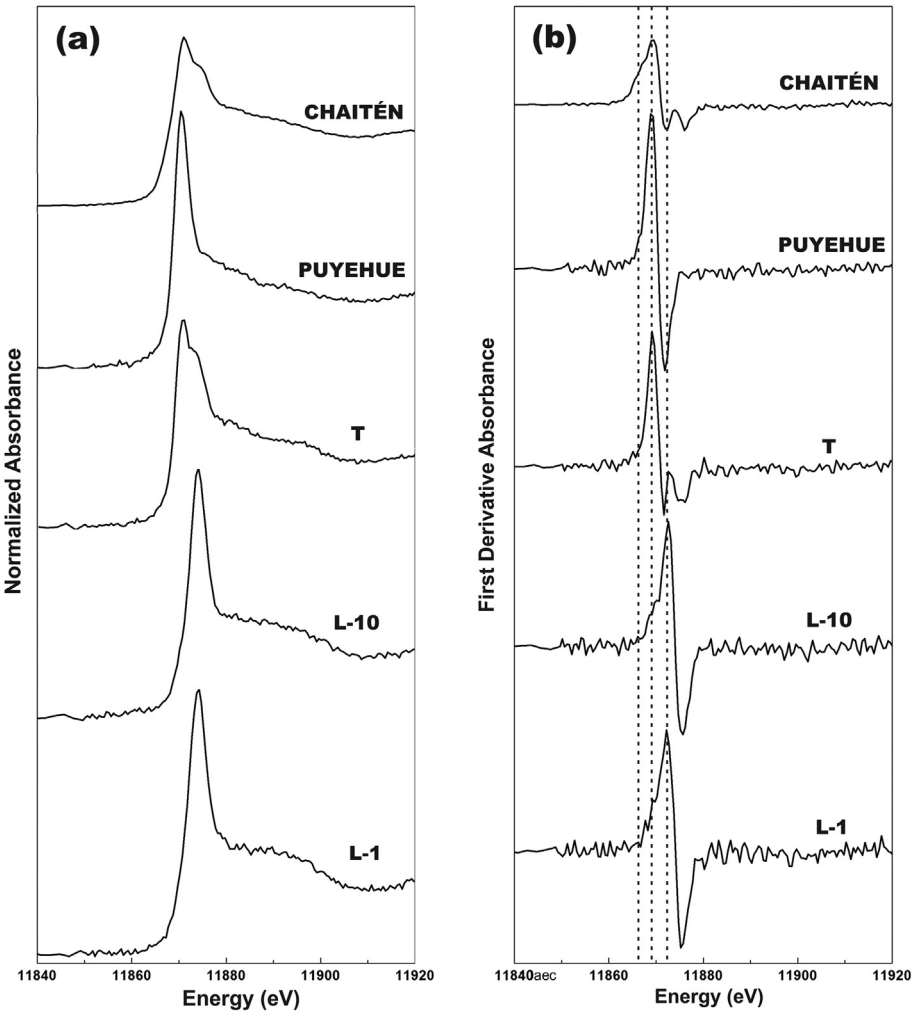

Fig. 1. Normalized As K-edge XANES and their corresponding first derivative spectra for the studied samples. The dashed lines serve as a reference to identify changes in peak positions.

peak energies vary with the redox state of As, shifting towards higher energy values at increasing As oxidation state (e.g.: see Fig. SI2).

As seen in Fig. 1, both ancient and recent volcanic ashes are dominated by the presence of As(III). The first derivative shows that E_0 values in the Puyehue and Chaitén ashes are similar to that of the As(III) oxide reference material (Table 2). In the case of the Chaitén ash, a small shoulder at 11865.7 eV is also detected (Fig. 1a, Table 2) which indicates the presence of the most reduced species, As(-1). XANES spectra of the ancient ash shows two peaks that coincide with the positions of As(V) and As(III) reference materials (Fig. 1b, Table 2). Like recent ashes, the position of the more intense signal corresponds to an As(III) oxide.

The first derivative of loess samples showed the presence of two peaks that reveals two inflection points. Unlike T, the more intense signal in loess is found at energy values typically assigned to As(V) species, while the weak shoulder at ~11,869 eV is likely associated with As(III) species (Fig. 1b and Table 2).

Fig. 2 shows the proportion of the identified As phases in the analysed samples calculated by LCF analysis. The residual factors (R) and χ^2 values (Table 3) provide a measure of the goodness of the fit. For the Puyehue sample, the best LCF suggests that As(III)-O is associated with a silicate phase (100%), while for the Chaitén and T samples, only 66% of As(III) is in association with this phase (Fig. 2 and Table 3). In these last samples, the remaining fraction of As (34%) is represented by an As sulphide (in Chaitén) and a As(V)-O species (in T). In loess samples, the LCFs shows that the As(V)-O associated with Fe-oxide is the dominant species (>91%) while the As(III)-O associated with a silicate phase has a much lower contribution.

3.2.2. Fe speciation

Normalized Fe XANES spectra and the corresponding first derivative analysis for Fe in loess samples and reference materials are shown in Fig. 3 and SI3, respectively. Peak positions are listed in Table 4. Edge features among

Table 2
First derivative XANES peaks (in eV) for the studied samples and As reference materials. The spectra are available in SI2.

Reference materials								
Native As	As sulphides	As (II/III) sulphides		As (III)-O		As (III)-O in silicates	As(V)-O	
	Arsenopyrite	Orpiment	Realgar	Arsenolite	Na-arsenite	Macusaniglass	Na-arsenate	As (V)-Fe-oxide
11865.8	11865.6/ 11873.0	11866.6	11867.6	11869.0	11869.1	11869.0	11872.2	11872.7
Studied samples								
Recent volcanic ashes								
Chaitén	11865.7/ 11873.7			11869.4				
Puyehue				11869.1				
Ancient volcanic ashes								
T				11869.3			11872.6	
Loessic sediments								
L-1				11869.2			11872.2	
L-10				11869.9			11872.6	

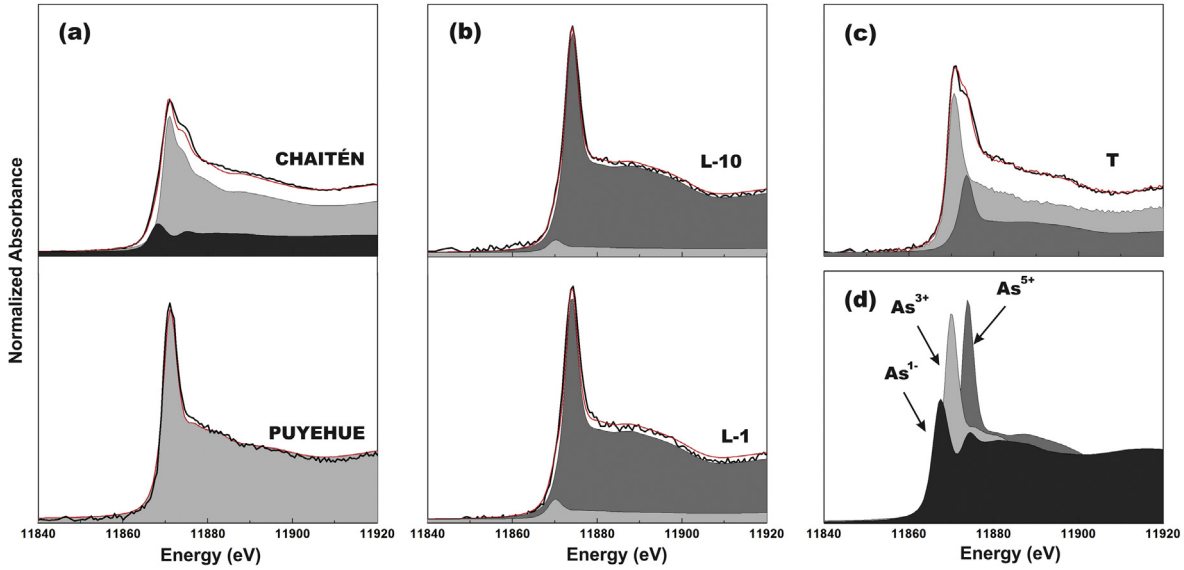

Fig. 2. Linear combination fits to As K-edge spectra of (a and c) recent and ancient volcanic ashes and (b) loess sediments. (d) As XANES spectra of As(-1)-S in arsenopyrite, As(III)-O in silicates glass and As(V)-coprecipitated on Fe oxy(hydr)oxides compound. Thick solid lines depict measured spectra, red solid lines indicate fit results. Black, light gray and dark gray fill indicate the contribution of As(1)-S, As(III) in silicates glass and As(V)-O species, respectively. The quantitative data for the fittings are provided in Table 3. All the reference compounds mentioned in Table 2 and Fig. SI2 has been considered in the LCF analysis as a reference compound.

Fe compounds in sulphide phases (e.g.: pyrite, marcasite and arsenopyrite), oxides/oxy(hydr)oxides (e.g.: goethite and ferrihydrite) and phyllosilicate phases (e.g.: illite and smectite) are very similar (O' Day et al., 2004). However, there are some distinctive spectrum characteristics between the Fe compounds groups that may help to differentiate them. For instance, pyrite has the pre-edge peak inflection at 7112.1 eV, whereas the pre-edge position in goethite, scorodite and illite is at ~7113 eV (Fig. SI3 and Table 4). Even though illite and goethite have the same pre-edge peak inflection position, they both have another primary peak at 7123.6 and 7124.5 eV, respectively (Table 4). When comparing the spectra of the loess samples with those of the Fe oxy(hydr)oxides and phyllosilicates, some similarities can be observed (Fig. 3 and Table 4). This suggests that these minerals are likely the dominant Fe phases in loess samples in concordance with previous mineralogical descriptions (Borgnino et al., 2013; García et al., 2014).

Table 3
Results of linear combination fits applied to As K-edge XANES spectra of volcanic ashes and loess sediments samples.

Samples	LCF - XANES[a]			Statistical parameters	
	As[1– b]	As(III)-O in silicates[c]	As(V)[d]	*R factor*	χ^2
Recent volcanic ashes					
Chaitén	33.8 (0.9)	66.2 (0.9)		0.00095	0.141
Puyehue		100		0.00433	0.716
Ancient volcanic ash					
T		66.4 (0.9)	33.6 (0.9)	0.00115	0.193
Loessic sediments					
L-1		8.8 (0.2)	91.2 (0.2)	0.00367	0.687
L-10		5.8 (0.8)	94.2 (0.8)	0.00168	0.284

Values between parenthesis correspond to the standard deviation.
[a] Fitting range [11,840–11,920] eV for all cases.
[b] Natural arsenopyrite (FeAsS).
[c] Rhyolitic peraluminous glassspectrum from Macusani (SEPeru), obtained from Borisova et al. (2010).
[d] As(V) co-precipitated on Fe oxy(hydr)oxides and analytical reagents Na-arsenate ($Na_2HAsO_4{\cdot}7H_2O$).

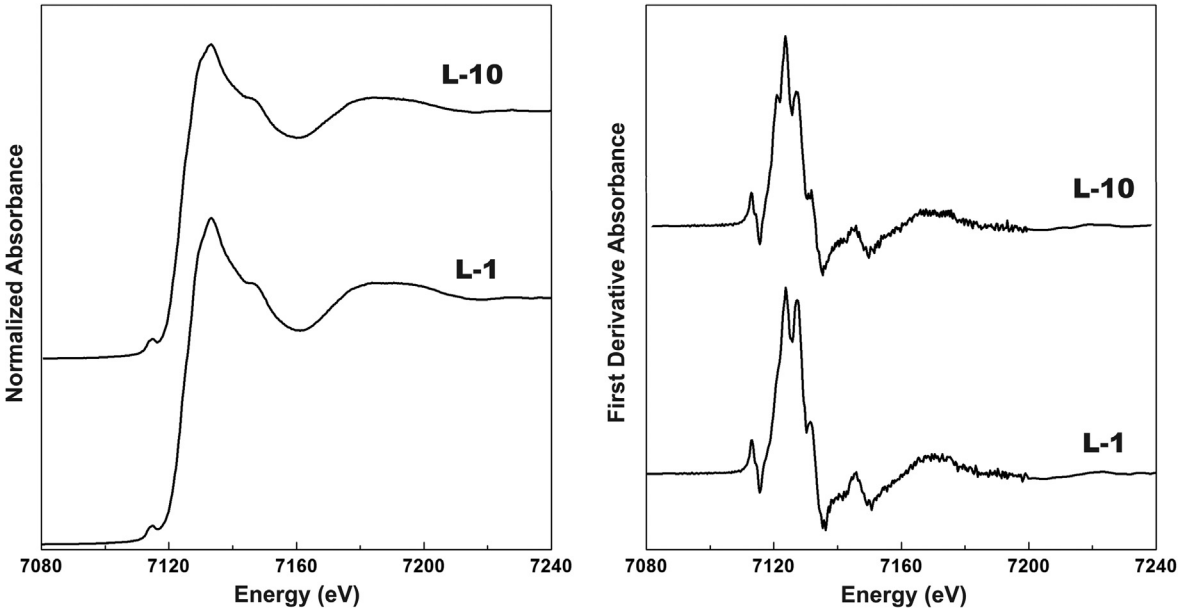

Fig. 3. Normalized Fe K-edge XANES and their corresponding first derivative spectra for studied samples.

Moreover, LCFs performed on Fe spectra (not shown) revealed that Fe oxy(hydr)oxides are dominant and contributed more than 90% of the Fe present in the samples.

3.3. EXAFS analysis

3.3.1. As coordination

Fig. 4 shows the corresponding k^3-weighted EXAFS spectra for the studied samples and reference materials, while the derived structural parameters are listed in Table 5. As seen in this figure, EXAFS spectra are noisy due to the low As concentrations. However, the proposed EXAFS model for the Puyehue ashes resembles an AsO_3 pyramidal-like structure (Pokrovski et al., 1999, 2002; Tossel and Zimmermann, 2008) composed of three oxygen atoms at a distance of 1.79 Å around As atom (Table 5). This arrangement is similar to that defined for the reference material, As_2O_3. Beyond the first shell, the EXAFS model gives reasonable fit with Na, Si and Al atoms as probable second neighbor (Table 5), suggesting that the As(III)-O species are included within the glass network structure through chemical bonding with Al/Si, or electrostatically bonded with cations. The best fit obtained for the Chaitén EXAFS data resulted in a central As atom and three O atoms at 1.79 Å, which is the same distance obtained for the Puyehue sample. Additionally, the model proposes the presence of a central As atom associated with three atoms of Fe at 2.42 Å (Table 5). This arrangement coincides with the first-shell of As-Fe coordination reported by Foster et al. (1998) for As-bearing sulphides in partially oxidized tailings. In that work, the authors obtained a longer distance than the arsenian pyrite reported by Tingle et al.

Table 4
First derivative XANES peaks (in eV) for the studied samples and Fe reference materials.

Reference materials						
Sulfides						
Pyrite	7112.1	7117.7	7123.8	7130.1		
Oxides and (hydr)oxides						
Goethite	7113.1	7123.6	7128.4	7133.7	7137.3	7145.8
Scorodite	7113.4	7123.5	7128.4		7137.0	
Phyllosilicates						
Illite	7113.1	7124.5	7128.2	7131.4		7145.2
Studied samples						
L-1	7113.1	7123.7	7127.4	7131.5	7138.3	7145.6
L-10	7113.1	7123.7	7127.3	7131.7	7140.1	7145.5

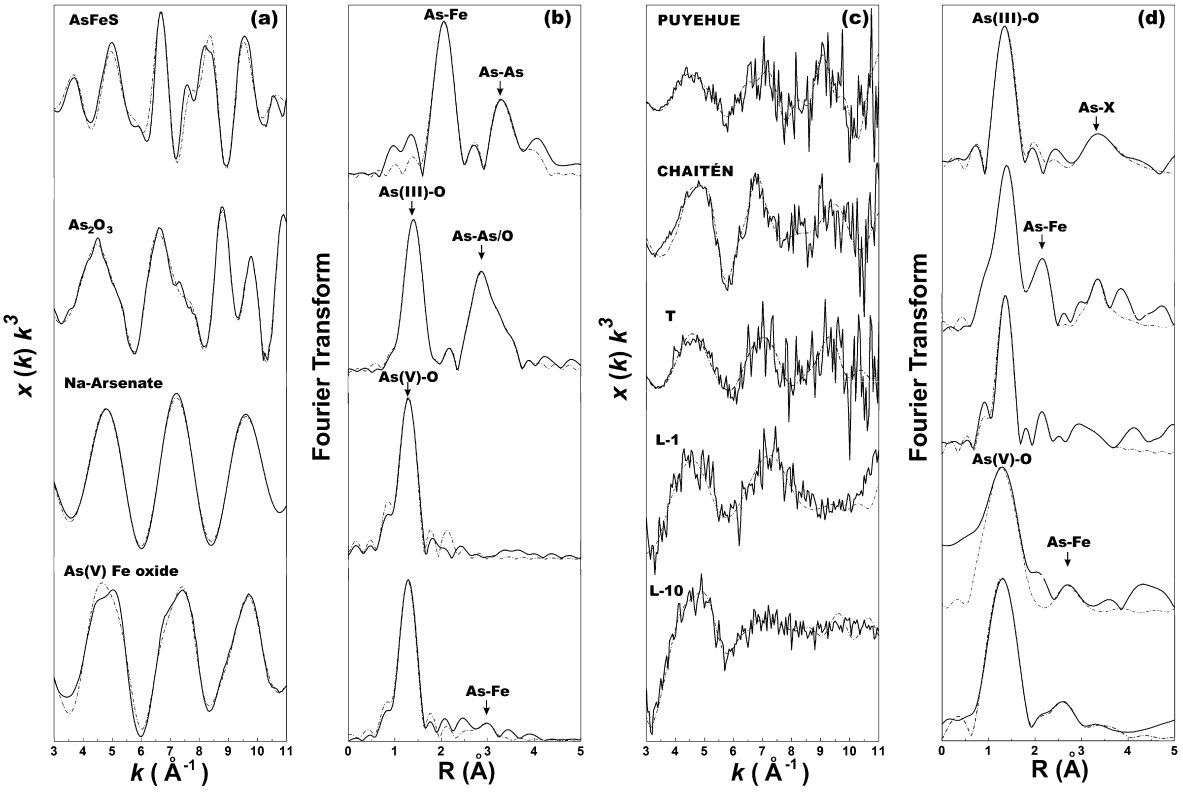

Fig. 4. Normalized k^3-weighted EXAFS spectra (a, c), and Fourier transform magnitudes at As K-edge (b, d) of volcanic ashes, loess sediments and As(-1), As(III) and As(V) reference materials (not corrected for phase shift). Solid lines represent experimental data; dashed lines correspond to fits obtained with parameters indicated in Table 5. As concentrations are in the range 2.4–40 μg g^{-1}.

(1996; 2.31 Å). According to Foster et al. (1998), the difference obtained in As-Fe distance may be due to the difficulties involved in fitting the strongly overlapped first- and second-shell features. In spite of these difficulties, the obtained results in EXAFS analysis were consistent with those obtained with LCF that revealed the presence of more than one oxidation state of As in the Chaitén sample. For the ancient volcanic ash, the EXAFS model revealed that the first neighbor around the central As atom is located at 1.75 Å with a $N \sim 3.2$. These parameters in the T sample are almost certainly the result of overlapping peaks between those of As(III)-O and As(V)-O species (1.79 Å in As_2O_3 and 1.69 Å in Na-Arsenate, see Table 5). Indeed, the As-O distance in the T sample (1.75 Å) is intermediate between the As(III)-O distance (1.79 Å) in recent ashes and As(V)-O distance in loess samples (1.69 Å). The same analysis applies to the N values (3.2, 3 and 4, respectively). Finally, in loess sediments the As first shell is found at ~1.69 Å with N ~4 (Table 5). This arrangement can be clearly assigned to the As in arsenates. The second shell is found at ~3.3 Å

Table 5
EXAFS fit results at the As K-edge for the studied samples, FeAsS, As(III) and As(V) reference materials. Experimental and calculated curves are plotted in Fig. 4.

Samples	Shell	N	R (Å)	σ^2 (10^{-3} Å^2)	ΔE_0 (eV)	R-factor
Reference materials						
FeAsS	As-S	1*(f)*	2.34 (0.01)	1.2 (0.2)	7.00	0.006
	As-Fe	3*(f)*	2.37 (0.01)	1.3 (0.4)		
	As-As	1*(f)*	3.07 (0.01)	1.1 (0.2)		
	As-As	2*(f)*	3.19 (0.02)	1.8 (0.5)		
	As-Fe	4*(f)*	3.79 (0.03)	1.8 (0.2)		
As_2O_3	As-O	3*(f)*	1.79 (0.02)	3.7 (0.2)	11.60	0.015
	As-O	3*(f)*	3.04 (0.02)	5.4 (0.9)		
	As-As	3*(f)*	3.27 (0.02)	4.4 (0.3)		
	As-O	3*(f)*	3.44 (0.03)	5.2 (0.6)		
	As-As	6*(f)*	3.98 (0.04)	11.3 (0.4)		
$Na_2HAsO_4{\cdot}7H_2O$	As-O	4*(f)*	1.69 (0.01)	2.1 (0.1)	6.56	0.012
As(V) Fe oxide	As-O	4*(f)*	1.68 (0.01)	0.9 (0.1)	6.79	0.024
	As-Fe	2*(f)*	3.30 (0.02)	1.3 (0.1)		
Recent volcanic ash						
Chaitén	As-O	3.0 (0.1)	1.79 (0.01)	2.56 (0.1)	11.40	0.027
	As-Fe	3.0 (0.1)	2.42 (0.02)	2.3 (0.1)		
	As-x	1.0 (0.1)	3.16 (0.02)	36.7 (0.1)		
Puyehue	As-O	3.0 (0.1)	1.79 (0.01)	2.39 (0.1)	11.19	0.029
	As-x	1.0 (0.1)	3.17 (0.02)	3.12 (0.1)		
Ancient volcanic ash						
T	As-O	3.2 (0.1)	1.75 (0.01)	2.74 (0.1)	12.45	0.032
	As-x	1.1 (0.1)	3.21 (0.02)	3.78 (0.1)		
Loessic sediments						
L-1	As-O	4.0 (0.1)	1.69 (0.01)	2.6 (0.1)	8.68	0.025
	As-Fe	2.0 (0.1)	3.26 (0.01)	2.4 (0.1)		
L-10	As-O	4.0 (0.1)	1.69 (0.01)	3.4 (0.1)	6.74	0.030
	As-Fe	2.0 (0.1)	3.32 (0.01)	1.6 (0.1)		

Fit parameters include: N, coordination number, R (Å), interatomic distance, σ^2 (Å^2), squared Debye-Waller factor, ΔE (eV), energy difference accounting for phase shift between overall experimental spectrum and FEFF calculation. Fit quality was estimated using R-factor.
(f) Fixed parameter. The coordination number was fixed to the corresponding crystallographic values.
(*x*) Represent Na/Si or Al.

(Table 5), which is close to the As-Fe distance reported for As(V)-O adsorbed onto iron oxy(hydr)oxides phases (Sherman and Randall, 2003).

3.3.2. Fe coordination

The corresponding k^3-weighted Fe EXAFS spectra for L-1 and L-10 samples and reference materials are shown in Fig. 5. Based on the results obtained from the first derivative analysis of the Fe XANES spectra, goethite and illite were used as reference materials in the Fe EXAFS model. The results indicate that, in both samples, the first coordination shell is composed of six O atoms around a central Fe, three of them located at a distance of 1.96 Å; the remaining three atoms at 2.06 Å. The second shell corresponds to Fe-Fe bonding, with $N = 2$ at a distance of 3.09 Å (Table 6). These features are similar to those of Fe oxy(hydr)oxides compounds, which are important constituents in these sediments (Borgnino et al., 2013).

4. DISCUSSION

Since the early work of Zoller et al. (1974) it has been well known that volcanic emissions contain important amounts of volatiles such as H_2O, CO_2, SO_2, H_2S, HCl, HF, and N_2, CO, CH_4 and H_2 in lower proportions. In addition, volcanic gases and aerosols are enriched in many elements including alkali, alkali-earth, transition and heavy metals. Because magmatic temperatures are high, these elements are in their volatile form in gaseous volcanic emanations worldwide.

In Latin America, the presence of As in volcanic regions is associated with volcanic gases and/or volcanic products forming the volcanic edifice ejected as solid particles during the eruption (López et al., 2012). In the former vapor phase, As is normally present in fumaroles as AsH_3, which is the most volatile inorganic compound. In contrast, arsenolite $(As_2O_3)_2$ is rare because it needs temperatures higher than 460 °C to enter into the gaseous phase. Pokrovski et al. (2002) determined that in a system containing As–H_2O–NaCl–H_2S (at temperature >500 °C and pressures up to 6 MPa) the preferential species into the vapor phase is As $(OH)_{3(g)}$. XAS spectra and LCF of Puyehue and Chaitén samples identify the presence of As(III)-O associated with a silicate phase. In addition, the Debye-Waller factor obtained is around 0.0023/6 Å^2 which is close to the value previously reported by Borisova et al. (2010) for the As $(OH)_3$ and $AsO(OH)_2^-$ species in solution (0.002 A^2). These σ^2 values, along with the similarity with the Macusani glass

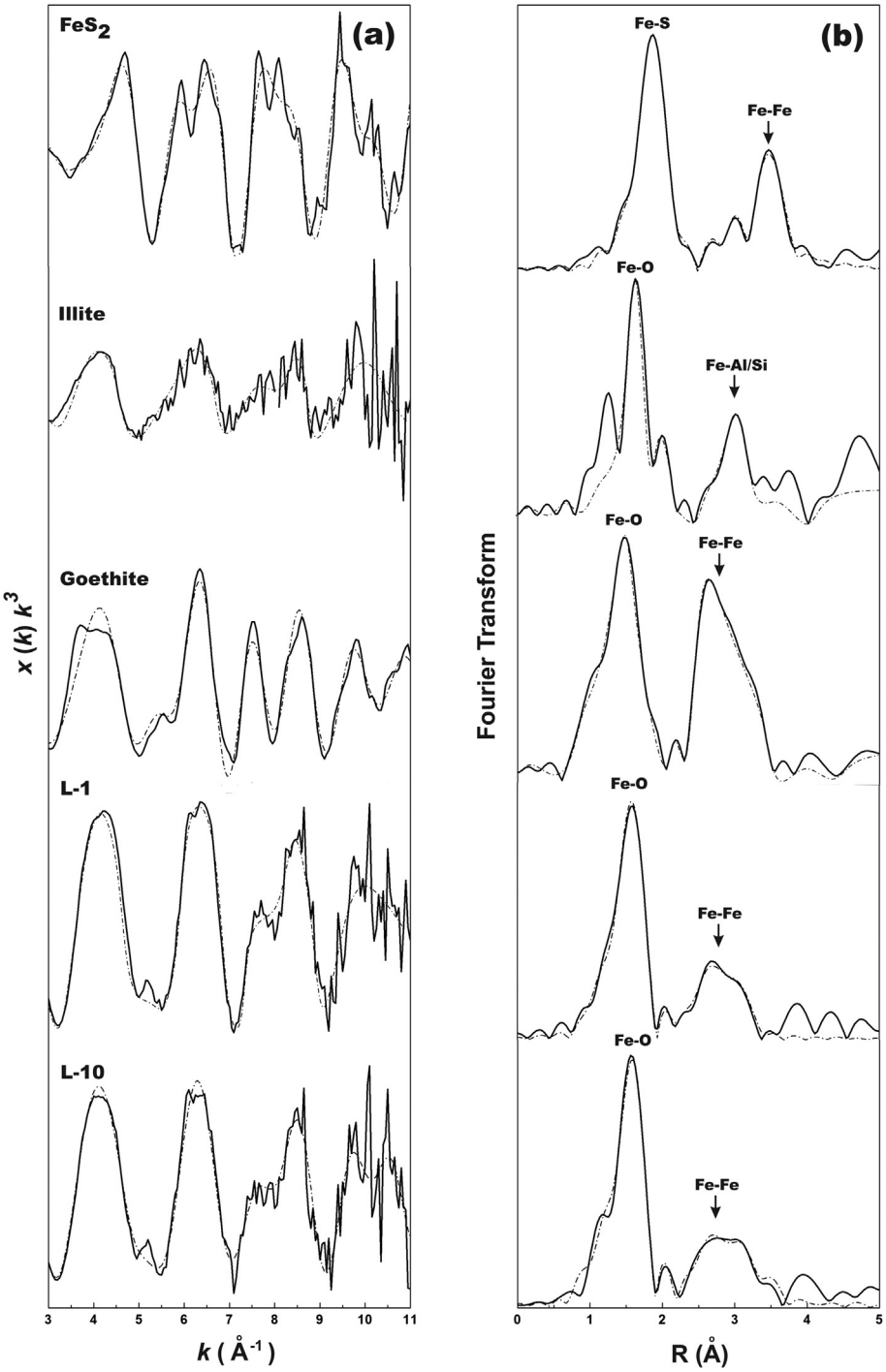

Fig. 5. (a) Normalized k^3-weighted EXAFS spectra, and (b) Fourier transform magnitudes at Fe K-edge of loess sediments and Fe reference materials. Solid lines represent experimental data; dashed lines correspond to fits obtained with the parameters indicated in Table 6.

XANES spectrum, strongly suggest that As(III) is present as the hydroxide species $As(OH)_3$ in both recent volcanic ashes, together with the corresponding deprotonated species, $AsO(OH)_2^-$. As a consequence of the in-plume conditions, it is likely that these As gaseous species would be adsorbed onto the glass particles or even incorporated within the mineral structure. Besides, at elevated pressures and water contents, the hydrous melt resembles an aqueous fluid (Shen and Keppler, 1997) which favors the incorporation of the As-oxy-hydroxide complex into the disordered melt (Farges et al., 2006).

The second neighbor (i.e., As chemically linked to Al/Si atoms or electrostatically bound to cations) was also explored by the analysis of EXAFS spectra. However, the

Table 6
EXAFS fit results at the FeK-edge for L-1 and L-10 sediments and Fe reference materials. Experimental and calculated curves are plotted in Fig. 5.

Samples	Shell	N	R (Å)	σ^2 (10^{-3} Å^2)	ΔE_0 (eV)	R-factor
Reference materials						
Pyrite	Fe-S	6 (*f*)	2.23 (0.01)	0.7 (1.1)	−1.1 (1.0)	0.018
	Fe-S	6 (*f*)	3.42 (0.01)	5.9 (2.2)		
	Fe-S	2 (*f*)	3.57 (0.02)	0.8 (3.9)		
	Fe-Fe	12 (*f*)	3.80 (0.02)	10.0(1.7)		
Goethite	Fe-O	3 (*f*)	1.95 (0.01)	3.2 (0.2)	1.4 (1.0)	0.021
	Fe-O	3 (*f*)	2.10 (0.01)	3.1 (0.4)		
	Fe-Fe	2 (*f*)	3.04 (0.02)	6.7 (0.1)		
	Fe-Fe	2 (*f*)	3.30 (0.01)	8.3 (0.5)		
Illite	Fe-O	6 (*f*)	2.04 (0.02)	6.1 (0.3)	2.1 (1.0)	0.034
	Fe-Al	3 (*f*)	3.06 (0.02)	7.8 (0.2)		
	Fe-Si	4 (*f*)	3.32 (0.02)	6.4 (0.3)		
Loessic sediments						
L-1	Fe-O	3.0 (0.1)	1.96 (0.02)	3.4 (0.3)	1.2 (1.0)	0.026
	Fe-O	3.0 (0.1)	2.06 (0.01)	2.9 (0.2)		
	Fe-Fe	2.0 (0.3)	3.09 (0.01)	5.2 (0.3)		
L-10	Fe-O	3.0 (0.1)	1.95 (0.02)	3.2 (0.5)	1.4 (1.0)	0.030
	Fe-O	3.0 (0.1)	2.07 (0.02)	3.0 (0.3)		
	Fe-Fe	2.0 (0.2)	3.11 (0.02)	6.0 (0.3)		

Fit parameters include: N, coordination number, R (Å), interatomic distance, σ^2 (Å^2), squared Debye-Waller factor, ΔE (eV), energy difference accounting for phase shift between overall experimental spectrum and FEFF calculation. Fit quality was estimated using R-factor. (*f*) Fixed parameter. The Coordination number was fixed to the corresponding crystallographic values.

low concentrations of As in the samples produced a noisy EXAFS spectrum and consequentially, the information about lattice coordination could not be accurately obtained. To overcome this, the information provided by chemical extraction procedures (see SI1) helped to constrain a possible model. After the total sample digestion, ~93% of As still remained in the residual fraction, suggesting that As is included within the glass network and thus, it must be strongly bound to Si/Al atoms. Although the disordered chemical structure of the glass should enhance the release of As, leaching experiments showed that at a circumneutral pH and after 14 days of ash-water interaction, only 6% of the total As is released from the studied samples (Bia et al., 2015).

Like Puyehue, the analysis of the Chaitén´s XAS spectra reveals the presence of As(III) within the glass structure. In addition to the As(III) species, XANES also discriminated the presence of As(-1) that likely corresponds to arsenian pyrite. The oxidation state of As in arsenian pyrite (Fe(S, As)$_2$) is controversial. Many authors have suggested a valence state of -1 for As, where As(-1) substitutes S in the S_2^{2-} unit to form Fe(As^{1-},S)$_2$ (Savage et al., 2000). Conversely, other authors have reported the presence of As(III) substituting Fe(II) in arsenian pyrite (Chouinard et al., 2005; Deditius et al., 2008). This latter association has been identified by X-ray photoelectron spectroscopy (XPS) in the uppermost surface of the studied ashes (Bia et al., 2015), while As(-1) was not identified. The exposure of the grain´s surface to the atmosphere may trigger the oxidation of the As(-1) in the arsenian pyrite to As(III), as it has been described in many previous works (e.g., Nesbitt et al., 1995; Corkhill and Vaughan, 2009).

The alteration of ashes is triggered by their interaction with water, atmospheric oxygen and CO_2. The weathering process of volcanic glass to allophane implies a series of steps that involves: (1) hydrolysis of the aluminosilicate glass leading to the formation of a solid product in the form of gibbsite-like sheets; (2) partial release of Si in the form of soluble monosilicic acid; and (3) development of a Si(OH)(O^{VI}Al)$_3$ structure as a result of the reaction between the gibbsite-like sheet and the monosilicic acid (Hiradate and Wada, 2005). The T sample has been exposed to the weathering agents for nearly 125 ka. XAS results reveal that the solid speciation of As in the ancient ash sample represents an intermediate stage between the As speciation determined in fresh ashes and in the loess samples. Like fresh ashes, the solid speciation of As in old tephras is dominated by the presence of As(III) atoms included within the Al-Si-glass structure. However, a minor proportion of As(V)-O species is also present. One interesting feature regarding this species is that the second shell of coordination is represented by a cation, likely Si, Al or Na with $N = 1$. This arrangement suggests that As(V) is coordinated within the Al-Si-glass lattice and not in the form of arsenate ions adsorbed onto Fe oxy(hydr)oxides. Therefore, the weathering of volcanic ashes should involve a rather slow (i.e., in the order of thousands of years) oxidation of the As(III) atoms in the most distal sites of the Al-Si network. In more advanced stages of weathering, the incongruent dissolution of the aluminosilicate glasses leads to the release of the As (either As (III) or As (V)) included in the glass network. Once in solution, As(III) oxidizes and forms arsenate ions. Depending on water pH, these ions could be adsorbed onto the Fe oxy(hydr)oxides that are usually present in sediments in

the form of amorphous coatings. This sequence explains the solid speciation of As in loess sediments, where a major proportion of As is in the form of As(V)-O, more specifically as arsenate sorbed onto Fe oxy(hydr)oxides. Regarding this, different surface complexes could develop when As (V) is adsorbed onto Fe oxides, each one characterized by known As–Fe distances (Arai et al., 2001; Ladeira et al., 2001; Sherman and Randall, 2003). The As-Fe distances calculated for loess samples range between 3.26 and 3.32 Å, which indicates that arsenate ions are adsorbed onto Fe oxy(hydr)oxides in the form of bidentate binuclear complexes.

5. CONCLUSIONS

For many years, the sources and processes that control the dynamics of As in groundwaters from the large Chaco-pampean region have been the subject of numerous studies. Although earlier works had already considered volcanic shards spread within the loess sediments that cover the entire plain to be the primary source of As, the solid speciation of this element in the volcanic materials and its transformations during weathering remained unknown.

One important challenge in the identification of the As solid speciation in the volcanic ashes and sediments here studied was related to their low total As concentrations (i.e., 2.4–40 $\mu g\ g^{-1}$), that determined low signal-to-noise ratios in the EXAFS data. In order to overcome this, a set of information derived from sequential extraction procedures, mineralogical determinations as well as qualitative and quantitative XANES analysis and EXAFS information was used to infer the coordination of As within the studied solids until the second shell. Beyond this, weak backscatterers were not evident in the EXAFS region, and therefore their identification in the silicate glass turned vague.

The results obtained in this work suggest that As atoms included within the aluminosilicate structure in natural glasses may be preserved for long periods of time in their original speciation, dominated by $As(OH)_3$ and $AsO(OH)_2^-$ complexes. The initial oxidation seems to occur within the glass lattice, as evidenced by the arrangement of As(V) atoms determined in the ~125 ka old ashes. When natural glasses are not preserved from weathering, such as in loess sediments, their alteration results in a slow release of the structural As atoms. The alkaline and oxidizing conditions that dominate the Chaco-pampean aquifers determine the formation of arsenate ions in solution and their subsequent adsorption onto Fe(hydr)oxide surfaces.

ACKNOWLEDGEMENTS

Authors wish to acknowledge the assistance of LNLS (Campinas-Brasil), CONICET and UNC (Argentina) for their support and the facilities used in this investigation. G. Bia acknowledges a doctoral fellowship from CONICET. L. Borgnino and M.G. Garcia are members of CICyT in Argentina´s CONICET. We thank the staff of the Laboratorio Nacional de Luz Sincrotron (LNLS), particularly to Dr. Santiago Figueroa for helpful discussions and technical assistance as well as Dr. Marcelo Zárate (INCITAP) for providing the tephra sample along with a detailed description of the sampling site. Authors gratefully acknowledge Dr. Gleb S. Pokrovski for his generous help with Macusani XAFS data. Language assistance by native English speaker Wendy Walker is also acknowledged. We are especially grateful to three anonymous reviewers for suggesting significant improvements to this manuscript.

APPENDIX A. SUPPLEMENTARY MATERIAL

Supplementary data associated with this article can be found, in the online version, at http://dx.doi.org/10.1016/j.gca.2017.06.016. These data include Google maps of the most important areas described in this article.

REFERENCES

Alexandratos V. G., Elzinga E. J. and Reeder R. J. (2007) Arsenate uptake by calcite: macroscopic and spectroscopic characterizationof adsorption and incorporation mechanisms. *Geochim. Cosmochim. Acta* **71**, 4172–4187.

Arriaza B., Amarasiriwardena D., Cornejo L., Standen V., Byrne S., Bartkus L. and Bandak B. (2010) Exploring chronic arsenic poisoning in pre-Columbian Chilean mummies. *J. Archaeol. Sci.* **37**, 1274–1278.

Arai Y., Elzinga E. J. and Sparks D. L. (2001) X-ray absorption spectroscopic investigation of arsenite and arsenate adsorption at the aluminum oxide–water interface. *J. Colloid Interface Sci.* **235**, 80–88.

Aurelio G., Fernández-Martínez A., Cuello G. J., Roman-Ross G., Alliot I. and Charlet L. (2010) Structural study of selenium (IV) substitutions in calcite. *Chem. Geol.* **270**, 249–256.

Baur W. H. and Khan A. A. (1970) On the crystal chemistry of salt hydrates. VI. The crystal structures of disodium hydrogen ortho arsenate heptahydrate and of disodium hydrogen orthophosphate heptahydrate. *Acta Cryst.* **26**, 1584–1596.

Byrne S., Amarasiriwardena D., Bandak B., Bartkus L., Kane J., Jones J., Yañez J., Arriaza B. and Cornejo L. (2010) Were Chinchorros exposed to arsenic? Arsenic determination in Chinchorro mummies' hair by laser ablation inductively coupled plasma-mass spectrometry (LA-ICP-MS). *Microchem. J.* **94**, 28–35.

Bhattacharya P., Claesson M., Bundschuh J., Sracek O., Fagerberg J., Jacks G., Martin R. A., Storniolo A. del R. and Thir J. M. (2006) Distribution and mobility of arsenic in the Rio Dulce alluvial aquifers in Santiago del Estero Province, Argentina. *Sci. Total Environ.* **358**, 97–120.

Bia G., Borgnino L., Gaiero D. and Garcia M. G. (2015) Arsenic-bearing phases in South Andean Volcanic ashes: Implications for As mobility in Aquatic environments. *Chem. Geol.* **393–394**, 26–35.

Borgnino L., Garcia M. G., Bia G., Stupar Y. V., Coustumer Ph. L. and Depetris P. J. (2013) Mechanisms of fluoride release in sediments of Argentina's central region. *Sci. Total Environ.* **443**, 245–255.

Borisova A. Y., Pokrovski G. S., Pichavant M., Freydier R. and Candaudap F. (2010) Arsenic enrichment in hydrous peraluminous melts: insights from femto second laser ablation inductively coupled plasma-quadrupole mass spectrometry, and in situ X-ray absorption fine structure spectroscopy. *Am. Mineral.* **95**, 1095–1104.

Bundschuh J., Farias B., Martin R., Storniolo A., Bhattacharya P., Cortes J., Bonorinod G. and Albouy R. (2004) Groundwater arsenic in the Chaco-Pampean Plain, Argentina: case study from Robles county, Santiago del Estero Province. *Appl. Geochem.* **19**, 231–243.

Bundschuh J., Litter M. I., Parvez F., Román-Ross G., Nicolli H. B., Jean J.-S., Liu C.-W., López D., Armienta M. A., Guilherme L. R. G., Gomez Cuevas A., Cornejo L., Cumbal L. and Toujaguez R. (2012) One century of arsenic exposure in Latin America: a review of history and occurrence from 14 countries. *Sci. Total Environ.* **429**, 2–35.

Chakraborty S., Bardelli F. and Charlet L. (2010) Reactivities of Fe(II) on calcite: selenium reduction. *Environ. Sci. Technol.* **44**, 1288–1294.

Chouinard A., Paquette J. and Williams-Jones A. E. (2005) Crystallographic controls on trace-element incorporation in auriferous pyrite from the Pascua epithermal high-sulfidation deposit, Chile-Argentina. *Can. Mineral.* **43**, 951–963.

Corkhill C. I. and Vaughan D. J. (2009) Arsenopyrite oxidation – a review. *Appl. Geochem.* **24**, 2342–2361.

Deditius A. P., Utsunomiya S., Renock D., Ewing R. C., Ramana C. V., Becker U. and Kesler S. E. (2008) A proposed new type of arsenian pyrite: composition, nanostructure and geological significance. *Geochim. Cosmochim. Acta* **72**, 2919–2933.

Elliot N. (1960) Interatomic distances in FeS2, CoS2 and NiS2. *J. Chem. Phys.* **33**, 903–905.

Essilfie-Dughan J., Hendry M. J., Warner J. and Kotzer T. (2013) Arsenic and iron speciation in uranium mine tailings using X-ray absorption spectroscopy. *Appl. Geochem.* **28**, 11–18.

Farges F., Linnen R. L. and Brown, Jr., G. E. (2006) Redox and speciation of tin in hydrous silicate glasses: a comparison with Nb, Ta, Mo, and W. *Can. Mineral.* **44**, 795–810.

Fernández-Martínez A., Cuello G. J., Jonson M. R., Bardelli F., Román-Ross G., Charlet L. and Turrillas X. (2008) Arsenate incorporation in gypsum probed by neutron, X-ray scattering and density functional theory modeling. *J. Phys. Chem. A* **112**, 5159–5166.

Foster A. L., Brown, Jr., G., Tingle T. N. and Parks G. A. (1998) Quantitative arsenic speciation in mine tailings using X-ray absorption spectroscopy. *Am. Miner.* **83**, 553–568.

Frechen M., Seifert B., Sanabria J. A. and Argüello G. L. (2009) Chronology of late Pleistocene Pampa loess from the Córdoba area in Argentina. *J. Quat. Sci.* **24**, 761–772.

Fuller C. C., Davis J. A. and Waychunas G. A. (1993) Surface-chemistry of ferrihydrite: Part 2. Kinetics of arsenate adsorptionand coprecipitation. *Geochim. Cosmochim. Acta* **57**, 227l–2282.

Fuess H., Kratz T., Töpel-Schadt J. and Miehe G. (1987) Crystal structure refinement and electron microscopy of arsenopyrite. *Z. Kristallogr.* **179**, 35–346.

García M. G., Borgnino L., Bia G. and Depetris P. J. (2014) Mechanisms of arsenic and fluoride release from Chacopampean sediments (Argentina). *Int. J. Environ. Health* **7**, 41–57.

Groat L. A., Evans R. J., Cempirek J., McCammon C. and Houzar S. (2013) Fe-rich and As-bearing vesuvianite and wiluite from Kozlov, Czech Republic. *Am. Mineral.* **98**, 1330–1337.

Gualtieri A. F. and Venturelli P. (1999) In situ study of the goethite-hematite phase transformation by real time synchrotron powder diffraction. *Am. Mineral.* **84**(5–6), 895–904.

Guggenheim S., Chang Y. H. and Vangroos A. F. K. (1987) Muscovite dehydroxylation high-temperature studies. *Am. Miner.* **72**(5–6), 537–550.

Hawthorne F. C. (1976) The hydrogen positions in scorodite. *Acta Crystallogr. A* **B32**, 2891–2992.

Hiradate S. and Wada S.-I. (2005) Weathering processes of volcanic glass to allophane determined by Al and Si solid state NMR. *Clay Clay Miner.* **53**, 401–408.

Kakoulli I., Prikhodko S. V., Fischer C., Cilluffo M., Uribe M., Bechtel H. A., Fakra S. C. and Marcus M. A. (2014) Distribution and chemical speciation of arsenic in ancient human hair using synchrotron radiation. *Anal. Chem.* **86**, 521–526.

Kröhling D. M. (1999) Sedimentological maps of the typical loessic units in North Pampa, Argentina. *Quatern. Int.* **62**, 49–55.

Ladeira A. C. Q., Ciminelli V. S. T., Duarte H. A., Alves M. C. M. and Ramos A. Y. (2001) Mechanism of anion retention from EXAFS and density functional calculations: arsenic (V) adsorbed on gibbsite. *Geochim. Cosmochim. Acta* **65**, 1211–1217.

Le Maitre R. W. (1984) A proposal by the IUGS Subcommission on the Systematics of Igneous Rocks for a chemical classification of volcanic rocks based on the total alkali silica (TAS) diagram. *Aust. J. Earth Sci.* **31**(2), 243–255.

López D., Bundschuh J., Birkle P., Armienta M. A., Cumbal L., Sracek O., Cornejo L. and Ormachea M. (2012) Arsenic in volcanic geothermal fluids of Latin America. *Sci. Total Environ.* **429**, 57–75.

Lorenzo F., Mehl A., Folguera A. and Zárate M. (2013) Sedimentology and stratigraphy of upper Miocene deposits from the transverse valleys of La Pampa province, Argentina. *Latin Am. J. Sedimentol. Basin Anal.* **20**, 67–84.

Nicolli H. B., Suriano J. M., Gómez Peral M. A., Ferpozzi L. H. and Baleani O. A. (1989) Groundwater contamination with arsenic and other trace elements in an area of the Pampa, Province of Córdoba, Argentina. *Environ. Geol. Water Sci.* **14**, 3–16.

Nicolli H. B., Bundschuh J., García J. W., Falcón C. M. and Jean J.-S. (2010) Sources and controls for the mobility of arsenic in oxidizing groundwaters from loess-type sediments in arid/semi-arid dry climates – evidence from the Chaco Pampean plain (Argentina). *Water Res.* **44**, 5589–5604.

Nicolli H. B., Bundschuh J., Blanco M. del C., Tujchneider O. C., Panarello H. O., Dapeña C. and Rusansky J. E. (2012) Arsenic and associated trace-elements in groundwater from the Chaco-Pampean plain, Argentina: results from 100 years of research. *Sci. Total Environ.* **429**, 36–56.

Nesbitt H. W., Muir I. J. and Pratt A. R. (1995) Oxidation of arsenopyrite by air and air-saturated, distilled water and implications for mechanisms of oxidation. *Geochim. Cosmochim. Acta* **59**, 1773–1786.

O' Day P. A., Rivera N., Root R. and Carroll S. A. (2004) X-ray absorption spectroscopic study of Fe reference compounds for the analysis of natural sediments. *Am. Mineral.* **89**, 572–585.

Pertlik F. (1978) Structure refinement of cubic As_2O_3 (arsenolite) with single-crystal data, Czechoslovak. *J. Phys.* **B28**, 170–176.

Pokrovski G., Bény J.-M. and Zotov A. V. (1999) Solubility and Raman spectroscopic study of As(III) speciation in organic compound-water solutions. A hydration approach for aqueous arsenic in complex solutions. *J. Solution Chem.* **28**, 1307–1327.

Pokrovski G. S., Zakirov I. V., Roux J., Testemale D., Hazemann J.-L., Bychkov A. Y. and Golokova G. V. (2002) Experimental study of arsenic speciation in vapor phase to 500 °C: implications for As transport and fractionation in low-density crustal fluids and volcanic gases. *Geochim. Cosmochim. Acta* **66**, 3453–3480.

Ravel B. and Newville M. (2005) ATHENA, ARTEMIS, HEPHAESTUS: data analysis for X-ray absorption spectroscopy using IFEFFIT. *J. Synchrotron Radiat.* **12**, 537–541.

Rivadeneira M., Santoro C. M. and Marquet P. A. (2010) Reconstructing the history of human impacts on coastal biodiversity in Chile: constraints and opportunities. *Aquatic Conserv: Mar. Freshw. Ecosyst.* **20**, 74–82.

Root R. A., Hayes S. M., Hammond C. M., Maier R. M. and Chorover J. (2015) Toxic metal(loid) speciation during weathering of iron sulfide minetailings under semi-arid climate. *App. Geochem.* **62**, 131–149.

Savage K. S., Tingle T. N., O' Day P. A., Waychunas G. A. and Bird D. K. (2000) Arsenic speciation in pyrite and secondary weathering phases, Mother Lode gold district. Tuolumne County, California. *Appl. Geochem.* **15**, 1219–1244.

Sayers D. E. (2000) Report of the International XAFS Society Standards and Criteria Commitee. <http://www.i-x-s.org/OLD/subcommittee_reports/sc/>.

Shen A. H. and Keppler H. (1997) Direct observation of complete miscibility in the albite-H_2O system. *Nature* **385**, 710–712.

Sherman D. M. and Randall S. R. (2003) Surface complexation of arsenic(V) to iron(III) (hydr)oxides: structural mechanism from ab initio molecular geometries and EXAFS spectroscopy. *Geochim. Cosmochim. Acta* **67**, 4223–4230.

Swift J., Cupper M. L., Greig A., Westaway M. C., Carter C., Santoro C. M., Wood R., Jacobsen G. E. and Bertuch F. (2015) Skeletal arsenic of the pre-Columbian population of Caleta Vitor, northern Chile. *J. Archaeol. Sci.* **58**, 31–45.

Smedley P. L., Kinniburgh D. G., Macdonald D. M. J., Nicolli H. B., Barros A. J. and Tullio J. O. (2005) Arsenic associations in sediments from the loess aquifer of La Pampa, Argentina. *Appl. Geochem.* **20**, 989–1016.

Smedley P. L. and Kinniburgh D. G. (2002) A review of the source, distribution and behaviour of arsenic in natural waters. *Appl. Geochem.* **17**, 517–568.

Sracek O., Novák M., Sulovský P., Martin R., Bundschuh J. and Bhattacharya P. (2009) Mineralogical study of arsenic-enriched aquifer sediments at Santiago del Estero, Northwest Argentina. In Natural Arsenic in Groundwater of Latin America. Occurrence, health impact and remediation. Interdisciplinary Book Series: "Arsenic in the Environment (eds. J. Bundschuh, M. A. Armienta, P. Birkle, P. Bhattacharya, J. Matschullat and A. B. Mukherjee), vol. **1**, (J. Bundschuh and P. Bhattacharya Series Editors). CRC Press/Balkema, Leiden, The Netherlands, pp. 61–68.

Tingle T. N., Waychunas G. A., Bird D. K. and O'Day P. A. (1996) X-ray absorption spectroscopy (EXAFS) of arsenic solid solution in pyrite, Clio Mine, Mother Lode Gold District, Tuolumne county. *Geol. Soc. Am. Abst. Programs* **28**, 518.

Tossel J. A. and Zimmermann M. D. (2008) Calculation of the structures, stabilities, and vibrational spectra of arsenites, thioarsenites, and thioarsenates in aqueous solution. *Geochim. Cosmochim. Acta.* **72**, 5232–5242.

Tripaldi A., Ciccioli P. L., Alonso M. S. and Forman S. L. (2010) Petrography and geochemistry of late Quaternary dune fields of western Argentina: provenance of aeolian materials in southern South America. *Aeol. Res.* **2**, 33–48.

Wang P., Liu Y., Menzies N. W., Wehr J. B., de Jonge M. D., Howard D. L., Kopittke P. M. and Huang L. (2016) Ferric minerals and organic matter change arsenic speciation in copper mine tailings. *Environ. Pollut.* **218**, 835–843.

Waychunas G. A., Rea B. A., Fuller C. C. and Davis J. A. (1993) Surface chemistry of ferrihydrite: Part 1. EXAFS studies of the geometry of coprecipitated and adsorbed arsenate. *Geochim. Cosmochim. Acta* **57**, 2251–2269.

Zabinsky S. I., Rehr J. J., Ankudinov A., Albers R. S. and Eller M. J. (1995) Multiple scattering calculations of X-ray absorption spectra. *Phys. Rev. B* **52**, 2995–3009.

Zárate M. A. (2003) Loess of southern South America. *Quater. Sci. Rev.* **22**, 1987–2006.

Zárate M. A. and Tripaldi A. (2012) The aeolian system of central Argentina. *Aeol. Res.* **3**, 401–417.

Zielinski R. A., Foster A. L., Meeker G. P. and Brownfield I. K. (2007) Mode of occurrence of arsenic in feed coal and its derivative fly ash, Black Warrior Basin, Alabama. *Fuel* **86**, 560–672.

Zoller W. H., Gladney E. S. and Duce R. A. (1974) Atmospheric concentrations and sources of trace metals at the South Pole. *Science* **183**, 198–200.

Associate editor: Mario Villalobos